

Journal of Materials Chemistry A

Accepted Manuscript



This is an *Accepted Manuscript*, which has been through the Royal Society of Chemistry peer review process and has been accepted for publication.

Accepted Manuscripts are published online shortly after acceptance, before technical editing, formatting and proof reading. Using this free service, authors can make their results available to the community, in citable form, before we publish the edited article. We will replace this *Accepted Manuscript* with the edited and formatted *Advance Article* as soon as it is available.

You can find more information about *Accepted Manuscripts* in the [Information for Authors](#).

Please note that technical editing may introduce minor changes to the text and/or graphics, which may alter content. The journal's standard [Terms & Conditions](#) and the [Ethical guidelines](#) still apply. In no event shall the Royal Society of Chemistry be held responsible for any errors or omissions in this *Accepted Manuscript* or any consequences arising from the use of any information it contains.

Varying the Microphase Separation Patterns of Alkaline Polymer Electrolytes

Chen Chen,^a Jing Pan,^{*ab} Juanjuan Han,^{ab} Ying Wang,^a Liang Zhu,^b
Michael A. Hickner,^{*b} and Lin Zhuang^a

^a*College of Chemistry and Molecular Sciences, Hubei Key Lab of Electrochemical Power Sources, Wuhan University, Wuhan 430072, China,* ^b*Department of Materials Science and Engineering, The Pennsylvania State University, University Park, PA 16802, USA*

jpan@whu.edu.cn, hickner@matse.psu.edu

ABSTRACT

Alkaline polymer electrolyte fuel cells (APEFCs) are a class of promising energy conversion devices that are attracting ever-growing attention from the academic and industrial energy technology communities. Considerable efforts have been made towards the development of better alkaline polymer electrolytes (APEs), and manipulating the balance between high ionic conductivity and low swelling degree is consistently one of the most important issues in APE design. Constructing hydrophilic/hydrophobic microphase-separated morphologies in APEs has long been accepted as an effective way to optimize the ionic conductivity of these materials. However, not all patterns of phase separation lead to high APE ion conductive efficiency. Here we compare two kinds of polysulfone-based APE materials (*i.e.* self-aggregated quaternary ammonium polysulfone (*a*QAPSF) and pendant quaternary ammonium polysulfone (*p*QAPSF)). Experiment and simulation observations unambiguously reveal the existence of distinctly different patterns of microphase separation in *a*QAPSF and *p*QAPSF. In *a*QAPSF, the hydrophobic side chains residing apart from the quaternary ammonium (QA) group help to build broad and percolated pathways, which contribute to boosting the ion conductive efficiency of the material. The *a*QAPSF membrane with IEC equal to 0.98 mmol/g shows ionic conductivity as high as 108.3 mS/cm at 80 °C. While in *p*QAPSF, the introduction of a side chain between the backbone and the cation pushes the QA group away from the backbone and helps to build strong hydrophobic networks, which results in limited development of efficient ionic channels. However, when doubling the IEC of *p*QAPSF to 2.04 mmol/g, the conductivity can be increased to 75.1 mS/cm at 80 °C, and the hydrophobic network restrains the swelling of *p*QAPSF effectively (swelling degree is 25.0% at 80 °C). These materials with obvious phase separation showed good chemical stabilities, and can be considered as competitive candidates for application in fuel cells.

1. Introduction

Proton exchange membrane fuel cells (PEMFCs) with advantages such as compact device structure, room-temperature startup, and high power and energy densities,¹⁻³ have been considered an ideal electric energy conversion technology for vehicles and portable devices.^{3,4} However, the inherent strong acidic environment in PEMFCs imposes the restriction that only some precious metals (*e.g.* Pt) can be used as efficient and stable catalysts in these systems. To a large extent, cost and resource concerns have impeded the large-scale commercialization of PEMFCs.⁵⁻⁷

To mitigate the use of precious-metal catalysts in fuel cells, the possibility of high-performance alkaline polymer electrolyte fuel cells (APEFCs) has been raised.^{6,8-13} In the last decade, preliminary reports toward the realization of practical APEFCs have emerged, which have attracted ever-growing attention from the energy community for creating low-cost fuel cell devices.¹⁴⁻¹⁹ Albeit promising, the development of APEFCs is far from mature. At the current stage, one of the most urgent missions in this field is to develop high-performance APEs, which are expected to possess high ionic conductivity, sufficient mechanical strength, good chemical stability, and robust anti-swelling performance.²⁰ However, developing such high-performance APEs has proven to be challenging. Generally, for common APEs (*e.g.* quaternary ammonium polysulfone (QAPSF)), high ionic conductivity is usually not compatible with a low swelling degree, since high conductivity is often achieved by raising the ion exchange capacity (IEC) of the material. This increase in ionic functionalization of the polymer increases the water content of the membrane and leads to a decline in the material's mechanical properties.²¹⁻²⁷

To date, a number of reports have demonstrated strategies to balance the ion conductivity and anti-swelling performance of ionic polymer membranes.^{14,16,28-34} Among these studies, inducing a hydrophilic/hydrophobic microphase-separated morphology in the material is considered to be an effective means to achieve high conductivity by building well-defined ionic channels in APEs.^{14,16,30,31} However, we have observed that microphase separation does not always benefit efficient ion conduction. Our previous study¹⁴ predicted that only some types of aggregation of hydrophilic/hydrophobic species, which are determined by the specific chemical

structure of the material, can achieve efficient ionic pathways in APEs.¹⁴

To study the effect of different micro-morphologies on the conductive efficiency of APEs, we compared several APEs all based on a polysulfone (PSF) backbone. Taking quaternary ammonium PSF (QAPSF, Figure 1a), a well-studied APE as a reference, two other candidate materials with additional side chains, *i.e.*, self-aggregated quaternary ammonium PSF (*a*QAPSF, Figure 1b) and pendant quaternary ammonium PSF (*p*QAPSF, Figure 1c) are compared.

2. Experimental

2.1 Materials

Polysulfone (Udel P-3500, Solvay Advanced Polymers, L.L.C., USA), chloromethylmethylether (Shanghai Quhua Chemical Reagent Co. Ltd, 99%), trifluoroacetic acid (Sinopharm Chemical Reagent Co. Ltd, 99%), zinc powder (Shanghai Chemical Reagent Co. Ltd, 95%), 1,2-dichloroethane (Shanghai Chemical Reagent Co. Ltd, 99%), glycidyltrimethylammonium chloride (GTMAC), ammonia solution (Shanghai Chemical Reagent Co. Ltd, content of NH₃: 25~28 wt%), n-hexylamine (Aladdin Chemistry Co. Ltd., 99%), trimethylamine (Shanghai Chemical Reagent Co. Ltd., 33% alcohol solution), N,N-dimethylformamide (DMF, Shanghai Chemical Reagent Co. Ltd, 99%), dimethyl sulfoxide (DMSO, Shanghai Chemical Reagent Co. Ltd, 99%), potassium hydroxide (Sinopharm Chemical Reagent Co. Ltd, 85%), hydrochloric acid (Sinopharm Chemical Reagent Co. Ltd, 37%) were used as received.

2.2 Synthesis

1-amino-2-hydroxy-3-trimethylammoniumpropane chloride (pSQA) and N,N-di-(2-hydroxy-3-trimethylammoniumpropane chloride) amine (pDQA): GTMAC (4 g) was dissolved in water (20 mL) to form a solution, and later added into an ammonia solution (13.2 mL) at room temperature. Then the reaction mixture was stirred for 4 h at 40 °C. After the reaction, the solvent and excess ammonia were removed on a rotary vacuum evaporator at 50 °C to yield the mixture of *pSQA* and *pDQA*.

pSQA ([NH₂CH₂CH(OH)CH₂N(CH₃)₃]⁺ Cl⁻) and *pDQA* ([CH₂CH(OH)CH₂N(CH₃)₃]⁺ Cl⁻)₂ NH) : ¹HNMR (300MHz, d⁶-DMSO): NH₂- in *pSQA*: δ 5.6-5.7 ppm, 2H; -CH(OH)- in

*p*SQA and *p*DQA: δ 4.0-4.3 ppm, 2H; -CH(OH)- in *p*SQA and *p*DQA: δ 3.5-3.6 ppm, 3H; -CH₂N⁺(CH₃)₃ in *p*SQA and *p*DQA: δ 3.4-3.5 ppm, 3H, and δ 3.2-3.3 ppm, 3H; -N⁺(CH₃)₃ in *p*SQA and *p*DQA: δ 3.26 ppm, 26H; -NH₂CH₂- in *p*SQA and -NH(CH₂)₂- in *p*DQA: δ 2.5-2.8 ppm, 6H; -NH- in *p*DQA: δ 1.94 ppm, 1H. The mole ratio of *p*SQA to *p*DQA was calculated to be 1:1.

Elemental analysis: The weight percentages of the elements C, H, and N were tested to be 43.99%, 9.86%, and 14.2%, thus the molar ratio of *p*SQA to *p*DQA was calculated to be close to 1:1.

Chloromethylation of polysulfone: Chloromethylated polysulfone (CMPSF) used in this study was synthesized following a procedure reported earlier.²² The chloromethylation process of PSF was carried out in a three-neck round-bottom flask with a mechanical stirrer. PSF (10 g) was dissolved in 1,2-dichloroethane (70 mL). After adding zinc powder (1 g) and trifluoroacetic acid (4 mL) into the solution, chloromethylmethylether (20 mL) was added dropwise. The solution was stirred for 3, 5, and 12 h at 30 °C to produce the CMPSF samples with a degree of functionalization (DF) of 0.5, 1.0, and 1.5, respectively. The DF was the number of chloromethyl groups per repeat unit of the polymer. The thus-obtained CMPSF samples were precipitated in methanol, washed several times with deionized water, and then dried in a vacuum oven for 24 h at 60 °C. Since the chloromethylmethylether is a highly efficient reagent for the synthesis of CMPSF, we decided to use it in the chloromethylation reaction, although some other methods are more environmentally friendly for this purpose.³²

Quaternary ammonium polysulfone (QAPSF): CMPSF (DF = 0.5) was dissolved in N,N-dimethylformamide (DMF) to form a 15 wt% solution, into which trimethylamine was added dropwise, followed by stirring at 40 °C for 1 h.

Synthesis of α QAPSF: CMPSF (DF = 1.0 or 1.5) was dissolved in DMF to form a 15 wt% solution, into which n-hexylamine (50 or 75 mol% of the repeat unit of PSF) was added dropwise, followed by stirring at 40 °C for 2.5 h. Afterwards, trimethylamine (100 mol% of the repeat unit of PSF) was added, followed by stirring at 40 °C for 1 h to prepare the α QAPSF solution.

Pendant-cation quaternary ammonium polysulfone (p QAPSF): CMPSF (DF = 0.5 or 1.0) was dissolved in dimethyl sulfoxide (DMSO) to form a 10 wt% solution, into which the mixture

of *p*SQA and *p*DQA (the reactive amine group was 150 mol% of the repeat unit of PSF) was added and stirred for 4 h at 50 °C to produce *p*QAPSF solution.

Membrane casting. The resulting APE solution was cast onto a clean, flat glass plate and dried in oven at 70 °C for 20 h and then further dried in a vacuum oven at 80 °C for 10 h.

Anion exchange of APE membranes: To replace the Cl⁻ anion in APE for OH⁻, the APE membrane was immersed in 1 mol/L KOH solution for 10 h. This process was repeated four times to ensure complete displacement. Finally, the APE membrane in the OH⁻ counterion form was repeatedly rinsed with deionized water until the pH of the residual water was neutral.

2.3 Measurements

¹H NMR: ¹H NMR (300 MHz) analysis was performed on a Varian Mercury VX-300 spectrometer using deuterated dimethyl sulfoxide ([D₆]DMSO) as the solvent and tetramethylsilane (TMS) as the internal reference.

Elemental analysis: A VarioEL III (Elementar, Germany) was used for analyzing the C, H, and N elemental content in the samples.

Ion exchange capacity (IEC): The IEC of the APE samples was determined by titration. A membrane (in OH⁻ form) was immersed in a standard hydrochloric acid solution (0.1 mol/L, 30 mL) for 48 h. The solution was then titrated with a standard solution of potassium hydroxide (0.1 mol/L) to pH = 7. The membrane was washed and immersed in deionized water for 24 h to remove any residual HCl, and then dried under vacuum at 45 °C for 24 h and weighed to determine the dry mass (in Cl⁻ form). The IEC of the membrane was calculated with eq 1:

$$IEC = \frac{n_{i(\text{H}^+)} - n_{f(\text{H}^+)}}{m_{\text{dry}(\text{Cl})}} \quad (1)$$

where $n_{i(\text{H}^+)}$ was the initial moles of protons in the HCl solution, $n_{f(\text{H}^+)}$ was the final moles of protons in the HCl solution determined by titration, and $m_{\text{dry}(\text{Cl})}$ was the mass of the dry membrane in Cl⁻ form.

Ionic conductivity: To measure the ionic conductivity of APEs, a fully hydrated membrane in OH⁻ form was assembled into a fuel cell test fixture with carbon electrodes. Fully humidified N₂ was fed during measurements to exclude the influence of CO₂. The OH⁻ conductivity of fully hydrated membrane with different IEC values was measured by two-probe

electrochemical impedance spectroscopy (EIS) using an AC impedance analyzer (IviumStat, Netherlands) with the frequency ranging from 1 Hz to 1 MHz and an oscillating amplitude of 10 mV. The ionic conductivity was calculated as:

$$\sigma = \frac{l}{R_{\text{mem}} \times A} \quad (2)$$

where l was the membrane thickness in cm, A was the electrode area in cm^2 , and R_{mem} was the high-frequency resistance in Ω .

Swelling degree and water uptake: In order to obtain the swelling degree (denoted as SD) and water uptake (denoted as WU), both the mass and the dimensions of the dry membranes (in Cl^- form, denoted as $X_{\text{hyd}(\text{Cl})}$ and $m_{\text{dry}(\text{Cl})}$) were first recorded. The membrane was then immersed in 1 mol/L KOH solution for 48 h to convert Cl^- into OH^- , and washed with deionized water for several times to remove the remaining KOH. The dimension $X_{\text{hyd}(\text{OH})}$ and the wet mass $m_{\text{hyd}(\text{OH})}$ of the membranes could be determined after wiping the excess water from the surface. Accordingly, the SD and the WU were calculated respectively by:

$$SD(\%) = \frac{X_{\text{hyd}(\text{OH})} - X_{\text{dry}(\text{Cl})}}{X_{\text{dry}(\text{Cl})}} \times 100 \quad (3)$$

$$WU(\%) = \frac{m_{\text{hyd}(\text{OH})} - m_{\text{dry}(\text{Cl})}}{m_{\text{dry}(\text{Cl})}} \times 100 \quad (4)$$

Hydration number measurement: The hydration number (λ) represents the ratio between the amount of water molecules and hydroxide ions in the APE, and was defined as follows:

$$\lambda = \frac{WU}{IEC \times M_{\text{H}_2\text{O}}} \quad (5)$$

where WU was the water uptake, IEC was the ion-exchange capacity in mol/g, and $M_{\text{H}_2\text{O}}$ was the molar mass of water, which equaled to 18.015 g/mol.

Transmission electron microscopy (TEM): QAPSF, aQAPSF, and pQAPSF solutions were cast to form thin films on a Cu grid followed by exchanging the anions with I^- by immersion of the APE-coated Cu grid in 1 M NaI solution. The samples were then subjected to TEM

observations. Images were collected on an ultrahigh-resolution transmission electron microscope (JEOL JEM-2010FEF) at an acceleration voltage of 200 kV.

Small-angle X-ray scattering (SAXS): SAXS curves of unstained dry chloride form membranes were obtained using a Rigaku (formerly Molecular Metrology) instrument equipped with a pinhole camera with an Osmic microfocus Cu K α source and a parallel beam optic. Typical counting times for integration over a multiwire area detector were 1 h with typical membrane thicknesses on the order of 100 μm . Measurements were taken under vacuum at ambient temperature on dry samples. Scattering intensities were normalized for background scattering and beam transmission.

Mechanical properties: The wet APE membranes were cut into a dumbbell shape (12 mm \times 3 mm in the test area) and tensile measurements were performed using an Instron-5866 (Norwood, MA) instrument at a crosshead speed of 5 mm/min at room temperature (25 $^{\circ}\text{C}$).

Thermogravimetric analysis (TGA): TGA was performed on a TGA Q50 (TA Instruments, New Castle, DE) using samples (5 mg) placed in an Al $_2$ O $_3$ crucible. The samples were heated from 30 $^{\circ}\text{C}$ to 650 $^{\circ}\text{C}$ at a rate of 5 $^{\circ}\text{C}/\text{min}$ under flowing nitrogen (40 mL/min).

Chemical stability test: Membrane stability tests were conducted by immersing a piece of an APE membrane sample (50 \pm 5 μm in thickness) in 1 M NaOH solution. The solution was maintained at 80 $^{\circ}\text{C}$ for 30 days with replacement of the 1 M NaOH after every 3 days during the testing period. Periodically during the stability test, the IEC and ionic conductivity of APEs were tested to evaluate the changes of the materials under strong alkaline degradation conditions.

Membrane-electrode assembly and fuel cell test: Pt/C (60%, Johnson Matthey Co.) was mixed with a determined quantity of QAPSF (IEC = 1.02 mmol/g), *a*QAPSF (IEC = 0.98 mmol/g), or *p*QAPSF (IEC = 2.04 mmol/g) ionomer solution, and sprayed onto each side of QAPSF (IEC = 1.02 mmol/g), *a*QAPSF (IEC = 0.98 mmol/g), or *p*QAPSF (IEC = 2.04 mmol/g) membrane (55 \pm 5 μm in thickness), respectively, to produce the catalyst-coated membrane (CCM). The Pt loading of both the anode and the cathode was 0.4 mg/cm 2 , and the area of the electrodes was 4 cm 2 . The weight percentage of APE in both the anode and the cathode were calculated to be 20 wt%. The resulting CCM were pressed between two pieces of carbon cloth (CeTech W1S1005) to form the membrane electrode assembly (MEA).

The H₂-O₂ fuel cells were tested (850e Multi Range, Scribner Associates Co.) under galvanic mode using fully-humidified H₂ and O₂ gases flowing at 250 mL/min and a temperature of 60 °C with 0.1 MPa of back pressure.

3. Simulation

3.1 System construction

A coarse-grained (CG) model³⁵ was employed to describe the APE system at different hydration numbers λ . In this study, we designed five types of beads: backbone segment (BB), side chain segment (SC), quaternary ammonium ion (QA), hydrated hydroxide ion (OH), and water cluster (WT). As shown in Figure 2, all APE monomers consisted of 12 BB beads, and both QAPSF and *a*QAPSF monomers (IEC = 1.0 mmol/g) contained one QA bead and one OH bead, whereas the *p*QAPSF (IEC = 2.0 mmol/g) monomer contained three QA beads and three OH beads. These numbers are chosen according to the specific polymer structure from the experiments, and a detailed mapping method will be discussed below. Certain numbers of SC beads were placed according to the structures depicted in Figure 2. The system size, including the length of a polymer chain and the amount of polymer chains in a periodic box, was adjusted and optimized (following a protocol reported in the literature¹¹), such that simulation results were reproducible and calculated structure factors were consistent across multiple simulations. Finally, we chose a moderate system containing 800 polymer chains, each consisting of 10 monomers. In the case of a wet system, an additional 32000 WT beads were incorporated for QAPSF and *a*QAPSF corresponding to a hydration number of $\lambda = 20$, whereas an additional 48000 WT beads were incorporated for *p*QAPSF corresponding to the hydration number of $\lambda = 12$. The hydration number used here was determined by experiments with fully hydrated APE membranes. Such a configuration was adequate to generate reliable structural information (vide infra), while also avoiding simulating entanglement caused by using long polymer chains.³⁸

Here, we took the QAPSF system as an example to illustrate the mapping method. When mapping the simulated APE model to the QAPSF system, 12 BB beads (i.e., the backbone of a simulated APE chain) corresponded to two sulfone repeat units, a QA bead was a $-\text{NMe}_3^+$ group, an OH bead represented one hydroxide ion and three water molecules ($\text{OH}^- \cdot 3\text{H}_2\text{O}$), an SC bead

corresponded to a segment of linear chain ($-\text{CH}_2\text{NHCH}_2\text{CH}_2-$, $-(\text{CH}_2)_4-$, or $-(\text{CH}_2)_3\text{CH}_3$), and a WT bead represented four water molecules ($4\text{H}_2\text{O}$). Thus a dry system corresponded to $\lambda = 4$, and the wet system corresponded to $\lambda = 20$, the fully hydrated state of an APE (Table 1). The molecular weight (MW) of the simulated APEs was thus up to 86400 g/mol (200 sulfone repeat units), comparable to that of the experimental polysulfone (Udel P-3500, MW = 80000~86000 g/mol). The density of the simulated APEs (dry: 1.25 g/cm³ & wet: 1.13 g/cm³) was also in good agreement with the experimentally observed values (dry: 1.4 g/cm³ & wet: 1.1 g/cm³).

3.2 Force field

In this CG model,³⁵ beads were classified into four major types: polar (P), nonpolar (N), apolar (C), and charged (Q); and N and Q types were further divided into four subtypes according to their capability to form H-bond: “0” for no H-bond, “d” for H-bond donor, “a” for H-bond acceptor, and “da” for both H-bond donor and acceptor. In our system, the WT bead was set as “P”, OH bead “Qda”, QA bead “Q0”, SC bead “C”, and BB bead “Na”. Interactions between two beads included bonding, bending, non-bonded, and electrostatic interactions, which are briefly described in the following section.

The bonding interaction was described using Eq. 6. The force constant of the harmonic oscillator potential was $K_{\text{bond}} = 1250 \text{ kJ/mol}\cdot\text{nm}^2$, with an equilibrium distance $R_{\text{bond}} = 0.47 \text{ nm}$.

$$V_{\text{bond}}(R) = \frac{1}{2} K_{\text{bond}} (R - R_{\text{bond}})^2 \quad (6)$$

The bending interaction was described using Eq. 7. The basic equilibrium bond angle was $\theta_0 = 180^\circ$, and the force constant was set to $K_{\text{angle}} = 50 \text{ kJ/mol}\cdot\text{rad}^2$ for the rigid polysulfone backbone.

$$V_{\text{angle}}(\theta) = \frac{1}{2} K_{\text{angle}} \{\cos(\theta) - \cos(\theta_0)\}^2 \quad (7)$$

Non-bonded interactions between two beads (i and j) were described by a 12-6 Lennard-Jones (LJ) potential U_{LJ}

$$U_{\text{LJ}}(r) = 4\varepsilon_{ij} \left[\left(\frac{\sigma_{ij}}{r} \right)^{12} - \left(\frac{\sigma_{ij}}{r} \right)^6 \right] \quad (8)$$

where r was the distance between i and j , and σ_{ij} was the finite distance where the potential curve goes across the x axis at $U_{LJ} = 0$. For all LJ interactions the same $\sigma_{ij} = 0.47$ nm was used, and a cutoff distance $r_c = 1.2$ nm was chosen, corresponding to ca. 2.5σ . The LJ potential were smoothly shifted to zero between a distance $r_{\text{shift}} = 0.9$ nm and r_c in order to reduce the cutoff noise. Most of the interaction parameters (ϵ_{ij}) were set to the original value³⁵ as tabulated below, except that the BB-WT interaction was modified from the original value so as to mimic the hydrophilicity of QAPSF. The hydrophilicity of QAPSF could be characterized by the contact angle, whose experimental value was $55.1^\circ \pm 2.3^\circ$. If ϵ was set to 3.4 kJ/mol, the simulated contact angle was $70.7^\circ \pm 1.7^\circ$. Upon correcting the ϵ of BB-WT interaction to 3.9 kJ/mol, the simulation value was $55.4^\circ \pm 2.8^\circ$, which justified such a modification in ϵ .

Table 1. Interaction parameter, ϵ_{ij} (kJ/mol), used in the CGMD simulation.

Bead type	BB	SC	QA	OH	WT
BB	4.2				
SC	2.6	3.4			
QA	3.4	1.8	3.4		
OH	4.2	1.8	4.2	5.0	
WT	3.9*	1.8	5.0	5.0	5.0

*Modified from the original value (3.4 kJ/mol).

For electrostatic interactions, the original force field used a relative dielectric constant $\epsilon_r=20$ in Eq. 9,³⁵ which was applied in the simulation of wet systems. However, for the dry system where water molecules were present only in OH beads ($\text{OH} \cdot 3\text{H}_2\text{O}$), the ϵ_r should be reduced. We had carried out a series of simulations by tuning the ϵ_r from 1 to 20, and found that $\epsilon_r=5$ gave a structure factor most resembling to the experimental result of QAPSF.

$$U_{\text{el}}(r) = \frac{q_i q_j}{4\pi\epsilon_0\epsilon_r r} \quad (9)$$

3.3 Simulation process

In an NPT ensemble, the system was first heated from 300 K under 1 atm to 1000 K under 300 atm within 10 ns, and then annealed to 300 K under 1 atm for 50 ns. Such a high-temperature pretreatment was necessary to fully disentangle the polymer chains, and the high pressure was also needed to confine the system in the condensed state. After annealing, the

system was further equilibrated at 300 K under 1 atm for 10 ns, followed by a data production for 100 ns, during which a group of structural configurations were consecutively collected. In all simulations, a time step of 20 fs was chosen. The above simulation cycle was repeated for 9 times.

3.4 Software

All simulations were carried out using the LAMMPS code³⁶ and the system snapshots were produced using VMD.³⁷

4. Results and discussion

4.1 Synthesis and Characterization of APEs

The chemical structures of the synthesized samples were characterized by ¹H NMR. As is shown in Figure 3a, there were four chemical environments for the H atoms in the QAPSF membrane, the peaks between $\delta = 7.0$ to 8.5 ppm correspond to the H atoms in benzene ring, the single peak that emerges at $\delta = 1.6$ ppm is for the H in the methyl group of the quaternary carbon in the backbone, and the appearance of the peaks at $\delta = 4.5$ to 5.0 ppm identifies the H atoms of the benzyl group. More importantly, the peaks at $\delta = 3.1$ ppm demonstrate the existence of the QA ionic group in QAPSF. The ¹H NMR spectra of *a*QAPSF (Figure 3b) and *p*QAPSF (Figure 3c) are more detailed than that of QAPSF, due to the peaks emerging from the H atoms of the alkyl groups of the hydrophobic chains. In this work, by setting the DFs of CMPSF at specific values, QAPSF, *a*QAPSF, and *p*QAPSF with different calculated IECs (Table 1) were obtained. The experimental IECs measured by both ¹H NMR and titration methods (Table 1), were close to those calculated from the ideal chemical structures, demonstrating that the related reactions can be conducted effectively under the reported conditions.

4.2 Micro-morphologies of APEs

TEM observations were employed to collect visual information about the representative morphologies of different APEs. As can be identified from Figure 4, for QAPSF in which the cation is closely attached to the PSF backbone, the hydrophilic species are dispersed evenly in the dry film, suggesting no obvious microphase-separated morphology exists in the material.

This conclusion is supported by both TEM images (Figure 4a) and coarse-grained molecular dynamics (CGMD) simulation snapshots (Figure 4d) in which the hydrophilic domains are represented as dark regions and blue beads, respectively.

Interestingly, after introducing a side chain into the QAPSF system in different ways, the hydrophilic species in both *a*QAPSF (Figure 4b and e) and *p*QAPSF (Figure 4c and f) showed rather clear aggregation, although the microscopic morphologies in these two APEs were quite different. Specifically, in *a*QAPSF, the moderate-sized ionic clusters are distributed uniformly and connect well with each other (Figure 4b and e), whereas on the contrary, in *p*QAPSF the aggregated hydrophilic regions were distributed in the hydrophobic matrix with a relatively non-uniform pattern consisting of domains of different sizes (Figure 4c and f).

By comparing the CGMD simulation snapshots between the dry and wet states of the same APE system, it can be identified that the features of the micro-morphology in dry APEs are well preserved in the wet state. In QAPSF, the microphase separation is still not very clear in the hydrated state, and the hydrophilic domains are distributed uniformly in the polymer framework and connected to each other to some extent (Figure 4g). However, in *a*QAPSF, most of the swollen hydrophilic domains are connected with each other through “broadband” connections to form wide and well-connected hydrophilic channels. In the hydrated *a*QAPSF sample (Figure 4h), the hydrophobic species aggregate modestly and form isolated clusters. In contrast to *a*QAPSF, less aggregation of hydrophilic species can be observed in *p*QAPSF, and a hydrophobic network appears to form in the *p*QAPSF system. Apparently, the interconnected hydrophobic domains interrupt the connection of the narrow ionic channels to some extent in this sample (Figure 4i).

Quantitative information on the size of the ionic clusters can be obtained from experimental small-angle X-ray scattering (SAXS) patterns and structure factors from simulation. In Figure 5a, no ionic peak was observed in the SAXS signal of QAPSF (IEC = 1.02 mmol/g), which is in line with its features captured in TEM imaging (Figure 4a). For *a*QAPSF, sharp and narrow peaks emerged at 1.8 and 1.5 nm⁻¹ (corresponding to Bragg spacings of 3.5 and 4.2 nm) in SAXS and calculated structure factors (Figure 5) respectively, indicating the uniform aggregation of ionic clusters in the *a*QAPSF APE system. In comparison, for *p*QAPSF, shorter and broader peaks appeared at larger *q*-values of 2.3 and 2.1 nm⁻¹

(corresponding to a Bragg spacing of 2.7 and 3.0 nm) in SAXS and calculated structure factor patterns (Figure 5) respectively, indicating a less separated and non-uniform microphase morphology.

4.3 Conductive and swelling performance of APEs

The different micro-morphologies in APEs have a significant effect on the physicochemical properties of the samples. Figure 6a clearly shows that QAPSF (IEC = 1.02 mmol/g), which is a sample lacking microphase separation, exhibits low ionic conductivity and high swelling degree (see Figure 6a and Table 2). At a swelling degree of 12.1 and 56.2%, the conductivity of QAPSF (IEC = 1.02 mmol/g) is only 14.2 and 41.2 mS/cm (Figure 6a) at 30 and 80 °C, respectively.

Compared to QAPSF (IEC = 1.02 mmol/g), the conductivity and/or anti-swelling performance have been improved to different extents in *a*QAPSF versus *p*QAPSF. For *a*QAPSF, while the IEC increases from 0.98 to 1.27 mmol/g, the conductivities are 108.3 and 132.4 mS/cm at 80 °C, with swelling degrees of 19.5 and 51.6%. Different from that of *a*QAPSF, *p*QAPSF with a low IEC of 1.01 mmol/g shows a conductivity of 24.1 mS/cm at 80 °C, which is even lower than that of QAPSF (IEC = 1.02 mmol/g) with similar IEC. However, such a membrane demonstrates very low swelling. The swelling degree was just 6.7 % at 80 °C, 8 times less than that of QAPSF (IEC = 1.02 mmol/g). Increasing the IEC to 2.04 mmol/g improves conductive performance for *p*QAPSF, and the conductivity increases to 75.1 mS/cm while the swelling degree is limited to 25.0% at 80 °C.

It is widely accepted that both the microphase-separated morphology and IEC variation could contribute to the improvement of APE performance. Therefore, to unveil the independent role played by morphology in different APEs, we here employ both IEC-normalized conductivity (conductivity/IEC) and the hydration number (λ), to express the ion conductive efficiency and the water absorbing capacity per ion, respectively. As is shown in Figure 6b, the ion conductive efficiency of *p*QAPSF (IEC = 1.01 mmol/g) is lower than that of QAPSF (IEC = 1.02 mmol/g). Even when the IEC increases to 2.04 mmol/g, the conductive efficiency is similar to that of QAPSF (IEC = 1.02 mmol/g). In contrast, *a*QAPSF membranes exhibit much higher conductive efficiency than both of the other species, and the conductive efficiency for a

sample with 1.27 mmol/g IEC is slightly lower than that of the membrane with an IEC equal to 0.98 mmol/g. Such results provide evidence that the microphase-separated morphologies are not always good for the construction of effective ion conduction channels. The aggregated and well-connected hydrophilic species in *a*QAPSF indeed help to improve the efficiency of ion conduction. However, although there is also obvious microphase separation taking place in the case of *p*QAPSF, the aggregated but relatively isolated hydrophilic segments in *p*QAPSF do not contribute to the enhancement of ion conductive efficiency. The ions move rapidly within the large ionic domains that formed by the aggregated hydrophilic species, but the transport of the ions between the isolated hydrophilic clusters are hindered by the hydrophobic parts in *p*QAPSF films.

Fortunately, although the microphase-separated morphology in *p*QAPSF fails to bring enhanced ion conductive efficiency, the hydrophobic networks do contribute to improving the anti-swelling performance (Figure 6a). Figure 6c illustrates that, even though the IEC of *p*QAPSF (IEC = 2.04 mmol/g) is twice as large as that of QAPSF (IEC = 1.02 mmol/g) and *a*QAPSF (IEC = 0.98 mmol/g), the water absorbing capacity of the material is much lower than the other two APEs. At room temperature, there are just on average 12 water molecules for each cation in *p*QAPSF (IEC = 2.04 mmol/g, Table 1), and when the temperature is increased to 80 °C, the water uptake increases and leads to a higher hydration number (λ) of 24 water molecules per cation. This data compares to the λ of 23 and 22 at room temperature, and 115 and 40 at 80 °C for QAPSF (IEC = 1.02 mmol/g) and *a*QAPSF (IEC = 0.98 mmol/g), respectively.

4.4 Alkaline stability

Alkaline stability of APEs is a top concern since it determines the long-term performance of APE-based devices. The hydrophilic groups, which exhibit a strong electrophilic nature, are very likely to be attacked by OH⁻. The attack leads to chemical degradation of the material under alkaline conditions, especially at elevated temperatures. To evaluate the alkaline stability of QAPSF, *a*QAPSF, and *p*QAPSF, the membranes with different IECs were immersed in 1 M NaOH solution at 80 °C for 1 month with replacement of the 1 M NaOH every 3 days during the testing period. As shown in Table 3, poor chemical stability is observed for the QAPSF

membrane. After 30-days of immersion, the IEC and OH⁻ conductivity of QAPSF-1.02 decreased by 65.7% and 68.4%, respectively. In comparison, *a*QAPSF and *p*QAPSF exhibited much higher cation stability under alkaline degradation conditions. For *a*QAPSF films with initial IECs of 0.98 and 1.27 mmol/g, the IECs decreased to 0.81 and 0.90 mmol/g respectively after the stability test. Meanwhile, high OH⁻ conductivities of 85.6 and 91.4 mS/cm at 80 °C were maintained in the *a*QAPSF-0.98 and -1.27 membranes, which are 21.0 and 31.0% lower than the values measured for the samples, respectively, before the stability test. Since the chemical structure of the cations in *a*QAPSF and QAPSF are the same, the different cation stability observed in these two APEs must be due to the different morphologies. The hydrophobic side chains which induce obvious microphase separation may change the environment around the QAPSF chain, and potentially protect it from the severe nucleophilic attack by the hydroxide ion (Table 3). For *p*QAPSF, the improved chemical stability is attributed to the different chemical structure of the cations in such APEs. Previous studies have shown that alkyltrimethylammonium cations with proper alkyl chain length exhibited higher alkaline stability than that of the trimethylbenzylammonium group.³⁹ The IECs of *p*QAPSF-1.01 and -2.04 membranes decreased by just 11.9 and 15.2%, respectively, under the severe stability testing conditions, and the conductivities remained at 85.5 and 82.7% of their initial values, respectively, before the test (Table 3).

4.5 Fuel Cell Performance

Based on the above results, it seems reasonable to conclude that, although an obvious hydrophilic/hydrophobic microphase-separated morphology cannot guarantee superior ion conductive efficiency, microphase separation can still yield APEs with high conductivity by increasing the IEC of the material while controlling the water uptake. Meanwhile, the introduction of hydrophobic side chains in APE systems does improve the chemical and dimensional stabilities for the membranes. Higher ionic conductivity, lower swelling degree, and higher stabilities make APEs more suitable for fuel cell applications. Figure 7 summarizes the performance of assembled H₂-O₂ single cells using membranes with similar thickness (55±5µm) and Pt catalyst loading (0.4 mgPt/cm² in each side of anode and cathode) at a temperature of 60 °C. For an APEFC, the cell performance is closely related to the ionic

conductivity of the employed APE material. Higher conductivity leads to lower voltage drop, which ensures greater power density of the fuel cell. The peak power densities of the APEFCs using QAPSF-1.02 (the ionic conductivity was 29.9 mS/cm at 60 °C), *a*QAPSF-0.98 (the ionic conductivity was 82.9 mS/cm at 60 °C), and *p*QAPSF-2.04 (the ionic conductivity was 55.0 mS/cm at 60 °C) were 0.11, 0.61, and 0.36 W/cm² at the current densities of 0.20, 1.50, and 0.78 A/cm², respectively. In addition to the initial performance of the cells, we are also interested in the longevity of the APEFCs. It is hypothesized that fuel cells based on the APE which is more stable under alkaline ex-situ testing conditions should show higher stability during long-term operation in devices. However, we have not obtained such results which would demonstrate this point. A fuel cell is a complex system and its performance and durability are not only determined by the properties of the core materials (APE and catalysts), but also by the applied operational conditions, especially the management of water and possible generation of reactive oxygen species like peroxide and hydroperoxide that may degrade the materials locally. Subsequent work will be focused on the optimization of cell operation conditions to improve the long-term stability of the stable APEFCs.

5. Conclusions

In summary, we have compared the performance of different PSF-based APEs to evaluate how the patterns of their microphase-separated morphologies influence their materials behavior. Conventional QAPSF (IEC = 1.02 mmol/g) showed no obvious microphase separation and exhibited poor conductivity and high swelling. When introducing additional alkyl side chains into the QAPSF system by two different means, two kinds of APE materials (*a*QAPSF and *p*QAPSF) were realized, which show distinctly different patterns of phase-separated morphology. In *a*QAPSF, the aggregated hydrophilic species form broad and well-connected channels, significantly enhancing the ion conductive efficiency of the material and thus ensuring high ionic conductivity (0.1 S/cm at 80 °C) even when the IEC was as low as 0.98 mmol/g. In contrast in *p*QAPSF, the aggregated but relatively isolated hydrophilic domains cannot guarantee the efficient transport of hydroxide ions, but its strong hydrophobic networks make it possible for such an APE to achieve good conductive performance by increasing the IEC. The conductivity of *p*QAPSF with an IEC of 2.04 mmol/g is 75.1 mS/cm at 80 °C with a

swelling degree of 25.0%. Furthermore, *a*QAPSF and *p*QAPSF films exhibited much higher alkaline stability compared to the QAPSF membrane. High conductivities persisted in *a*QAPSF (IEC = 0.98 mmol/g) and *p*QAPSF (IEC = 2.04 mmol/g) after 30 days of stability test in 1 M NaOH solution at 80 °C. Higher conductivity and good anti-swelling performance as well as greater chemical stability of APEs promise better performance characteristics of alkaline fuel cells. The peak power densities of APEFCs based on QAPSF (IEC = 1.02 mmol/g), *a*QAPSF (IEC = 0.98 mmol/g), and *p*QAPSF (IEC = 2.04 mmol/g) were 0.11, 0.61, and 0.36 W/cm², respectively, at 60 °C.

ACKNOWLEDGEMENTS

This work is financially supported by the National Basic Research Program (2012CB215503, 2012CB932800), the National Natural Science Foundation of China (21303124, 21303123), and the Program for Changjiang Scholars and Innovative Research Team in University (IRT1030).

REFERENCES

1. J. R. Varcoe, P. Atanassov, D. R. Deke, A. M. Herring, M. A. Hickner, P. A. Kohl, A. R. Kucernak, W. E. Mustain, K. Nijmeijer, K. Scott, T. Xu, L. Zhuang, *Energy Environ. Sci.*, 2014, **7**, 3135-3191.
2. B. C. H. Steele, A. Heinzl, *Nature*, 2001, **414**, 345-352.
3. C.-Y. Wang, *Chem. Rev.*, 2004, **104**, 4727-4766.
4. M. Z. Jacobson, W. G. Colella, D. M. Golden, *Science*, 2005, **308**, 1901-1905.
5. S. Gu, R. Cai, T. Luo, Z. Chen, M. Sun, Y. Liu, G. He, Y. Yan, *Angew. Chem. Int. Ed.*, 2009, **48**, 6499-6502.
6. S. Lu, J. Pan, A. Huang, L. Zhuang, J. Lu, *Proc. Natl. Acad. Sci. U. S. A.*, 2008, **105**, 20611-20614.
7. J. R. Varcoe, R. C. T. Slade, *Fuel Cells*, 2005, **2**, 187-200.
8. S. Gu, W. Sheng, R. Cai, S. M. Alia, S. Song, K. O. Jensen, Y. Yan, *Chem. Commun.*, 2013, **49**, 131-133.
9. K. Asazawa, K. Yamada, H. Tanaka, A. Oka, M. Taniguchi, T. Kobayashi, *Angew. Chem.*,

- 2007, **119**, 8170-8173.
10. J. R. Varcoe, R. C. T. Slade, G. L. Wright, Y. Chen, *J. Phys. Chem. B*, 2006, **110**, 21041-21049.
 11. J. Pan, C. Chen, Y. Li, L. Wang, L. Tan, G. Li, X. Tang, L. Xiao, J. Lu, L. Zhuang, *Energy Environ. Sci.*, 2014, **7**, 354-360.
 12. N. Li, L. Wang, M. Hickner, *Chem. Commun.*, 2014, **50**, 4092-4095.
 13. N. Li, Y. Leng, M. A. Hickner, C.-Y. Wang, *J. Am. Chem. Soc.*, 2013, **135**, 10124-10133.
 14. J. Pan, Y. Li, J. Han, G. Li, L. Tan, C. Chen, J. Lu, L. Zhuang, *Energy Environ. Sci.*, 2013, **6**, 2912-2915.
 15. G. Li, J. Pan, J. Han, C. Chen, J. Lu, L. Zhuang, *J. Mater. Chem. A*, 2013, **1**, 12497-12502.
 16. M. Tanaka, K. Fukasawa, E. Nishino, S. Yamaguchi, K. Yamada, H. Tanaka, B. Bae, K. Miyatake, M. Watanabe, *J. Am. Chem. Soc.*, 2011, **133**, 10646-10654.
 17. K. Matsumoto, T. Fujigaya, H. Yanagi, N. Nakashima, *Adv. Funct. Mater.*, 2011, **21**, 1089-1094.
 18. N. J. Robertson, H. A. Kostalik IV, T. J. Clark, P. F. Mutolo, H. D. Abruña, G. W. Coates, *J. Am. Chem. Soc.*, 2010, **132**, 3400-3404.
 19. T. J. Clark, N. J. Robertson, H. A. Kostalik IV, E. B. Lobkovsky, P. F. Mutolo, H. D. Abruña, G. W. Coates, *J. Am. Chem. Soc.*, 2009, **131**, 12888-12889.
 20. J. Pan, C. Chen, L. Zhuang, J. Lu, *Acc. Chem. Res.*, 2012, **45**, 473-381.
 21. W. Li, J. Fang, M. Lv, C. Chen, X. Chi, Y. Yang, Y. Zhang, *J. Mater. Chem.*, 2011, **21**, 11340-11346.
 22. J. Pan, S. Lu, Y. Li, A. Huang, L. Zhuang, J. Lu, *Adv. Funct. Mater.*, 2010, **20**, 312-319.
 23. S. Gu, R. Cai, T. Luo, K. Jensen, C. Contreras, Y. Yan, *ChemSusChem*, 2010, **3**, 555-558.
 24. J. Wang, S. Li, S. Zhang, *Macromolecules*, 2010, **43**, 3890-3896.
 25. M. Tanaka, M. Koike, K. Miyatake, M. Watanabe, *Macromolecules*, 2010, **43**, 2657-2659.
 26. J. R. Varcoe, R. C. T. Slade, E. L. H. Yee, S. D. Poynton, D. J. Driscoll, D. C. Apperley, *Chem. Mater.*, 2007, **19**, 2686-2693.
 27. L. Wu, T. Xu, W. Yang, *J. Membr. Sci.*, 2006, **286**, 185-192.
 28. H. Liao, G. Xiao, D. Yan, *Chem. Commun.*, 2013, **49**, 3979-3981.
 29. N. Asano, M. Aoki, S. Suzuki, K. Miyatake, H. Uchida, M. Watanabe, *J. Am. Chem. Soc.*,

- 2006, **128**, 1762-1769.
30. J. Ran, L. Wu, X. Lin, L. Jiang, T. Xu, *RSC Adv.*, 2012, **2**, 4250-4257.
 31. N. Li, T. Yan, Z. Li, T. Thurn-Albrecht, W. H. Binder, *Energy Environ. Sci.*, 2012, **5**, 7888-7892.
 32. S. Gu, R. Cai, Y. Yan, *Chem. Commun.*, 2011, **47**, 2856-2858.
 33. J. Pan, Y. Li, L. Zhuang, J. Lu, *Chem. Commun.*, 2010, **46**, 8597-8599.
 34. L. Wu, T. Xu, D. Wu, X. Zheng, *J. Membr. Sci.*, 2008, **310**, 577-585.
 35. S. J. Marrink, A. H. de Vries, A. E. Mark, *J. Phys. Chem. B*, 2004, **108**, 750-760.
 36. S. Plimpton, *J. Comput. Phys.*, 1995, **117**, 1-19.
 37. W. Humphrey, A. Dalke, K. Schulten, *J. Mol. Graphics*, 1996, **14**, 33-38.
 38. L. M. Hall, M. E. Seitz, K. I. Winey, K. L. Opper, K. B. Wagener, M. J. Stevens, A. L. Frischknecht, *J. Am. Chem. Soc.*, 2012, **134**, 574-587.
 39. M. G. Marino, K. D. Kreuer, *ChemSusChem*, 2015, **8**, 513-523.

Figures

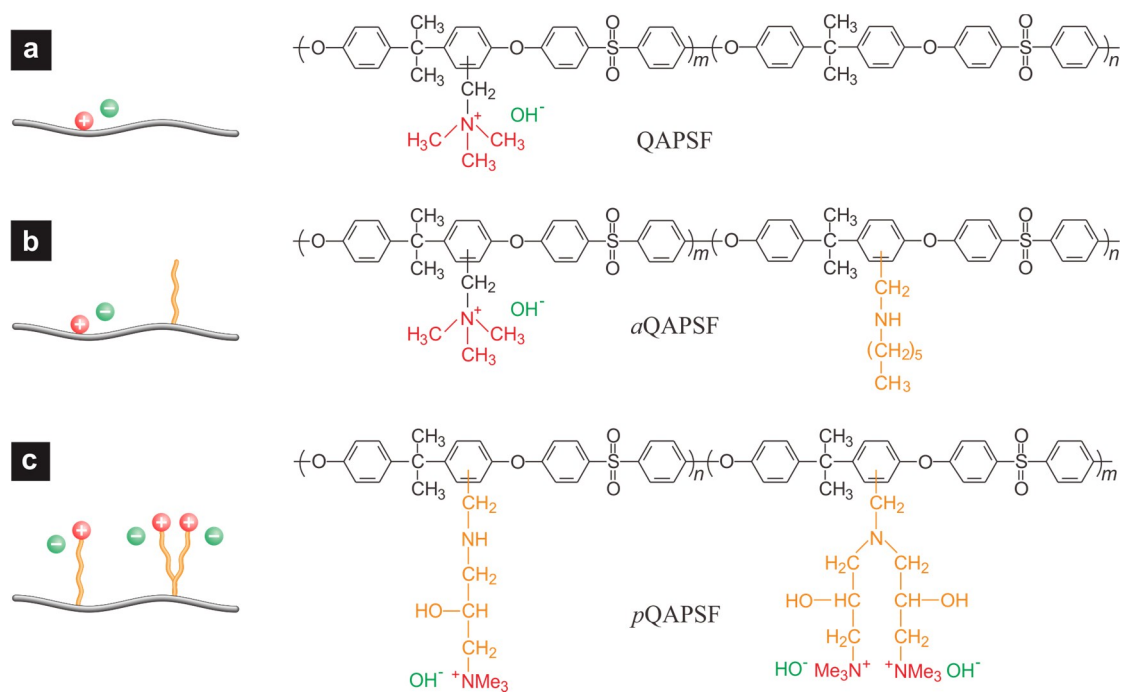


Figure 1. The schematic and chemical structures of (a) QAPSF, (b) *a*QAPSF, and (c) *p*QAPSF.

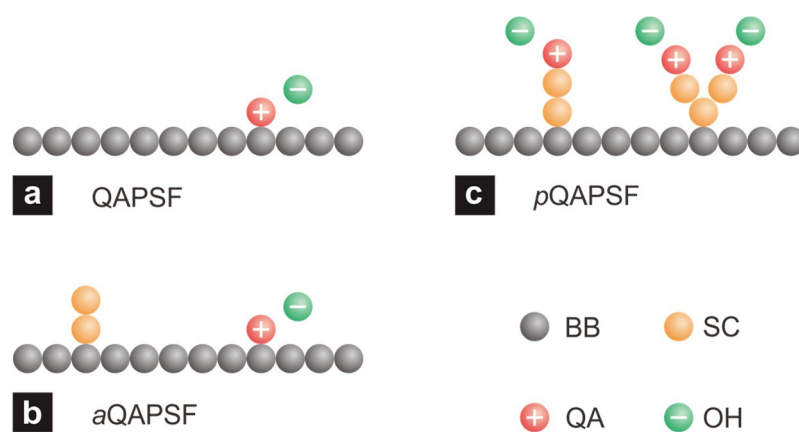


Figure 2. The monomer models for the simulated APEs: (a) QAPSF (IEC = 1.0 mmol/g), (b) *a*QAPSF (IEC = 1.0 mmol/g), (c) *p*QAPSF (IEC = 2.0 mmol/g). Four types of beads, backbone segment (BB), side chain segment (SC), quaternary ammonium ion (QA), and hydrated hydroxide ion (OH), were used as the building blocks to construct the APE systems. Note when mapping the above APE models to the quaternary ammonium polysulfone (QAPSF) system, one monomer corresponded to two sulfone repeat units.

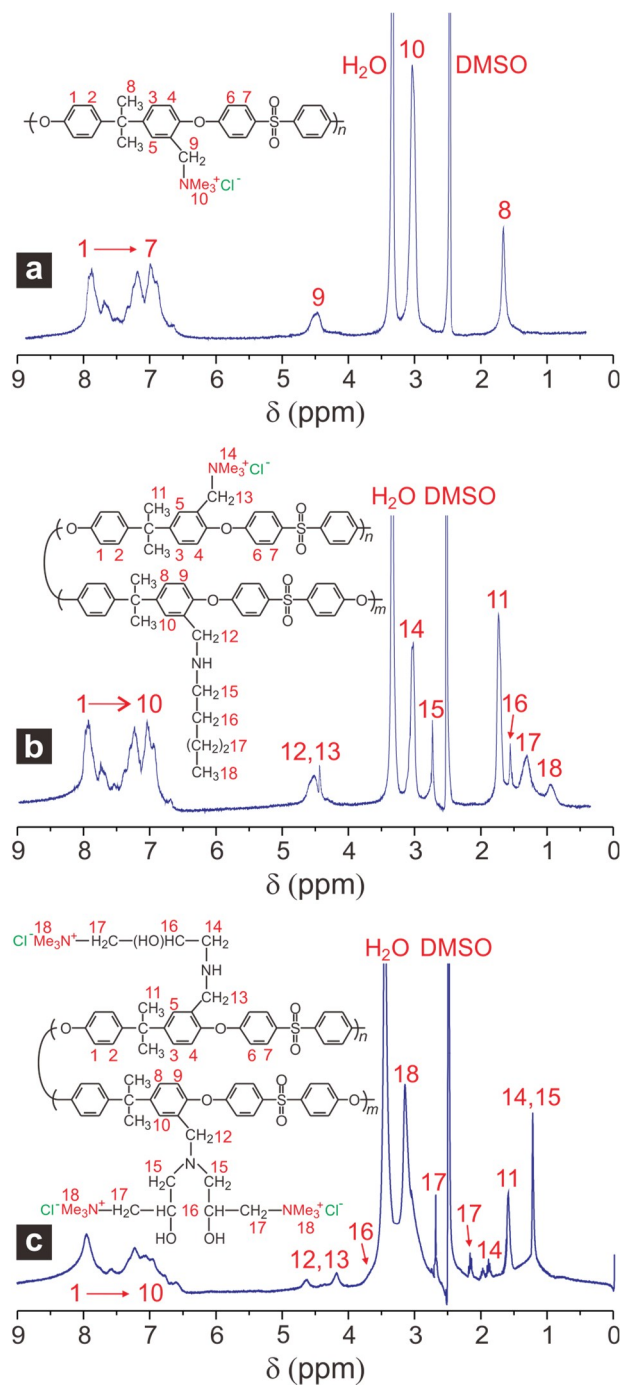


Figure 3. ¹H NMR spectra of (a) QAPSF, (b) aQAPSF, and (c) pQAPSF.

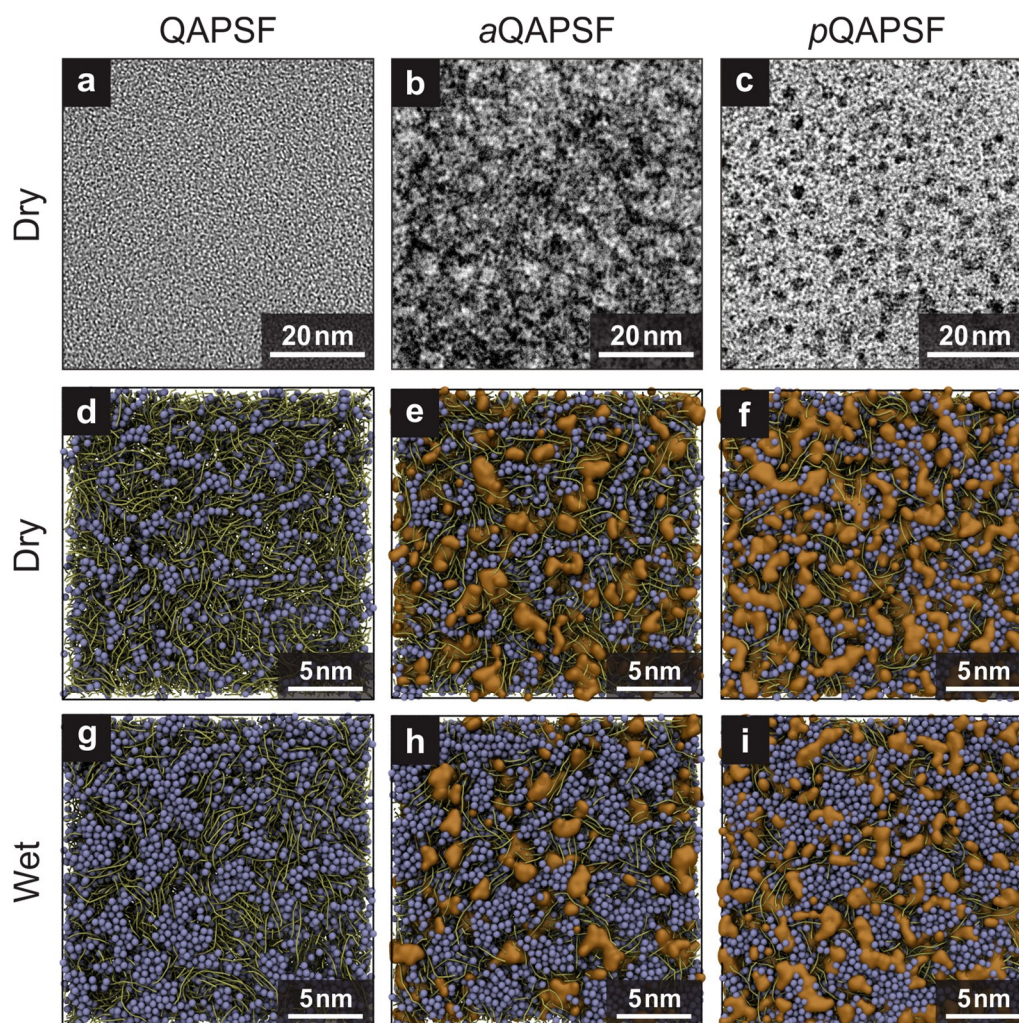


Figure 4. Microphase-separated morphology of different types of APEs. (a)-(c) Transmission electron microscopy (TEM) images for QAPSF (IEC = 1.02 mmol/g), *a*QAPSF (IEC = 0.98 mmol/g), and *p*QAPSF (IEC = 2.04 mmol/g), respectively. The dark spots in the images represented the hydrophilic domains dyed with iodine ions. (d)-(f) Snapshots taken from coarse-grained molecular dynamics (CGMD) simulations of QAPSF, *a*QAPSF, and *p*QAPSF in dry states. (g)-(i) Snapshots taken from CGMD simulations of QAPSF, *a*QAPSF, and *p*QAPSF in wet states. The unit cell had a length (*L*) of 22.9~27.0 (depending on the structure of the APE, and a cubic box of 22.0 nm in each dimension were shown here), and contained 800 polymer chains (yellow lines) with certain amount of hydrophilic species (blue beads, consisting of hydrated ions and water molecules) and additional side chains (orange domains).

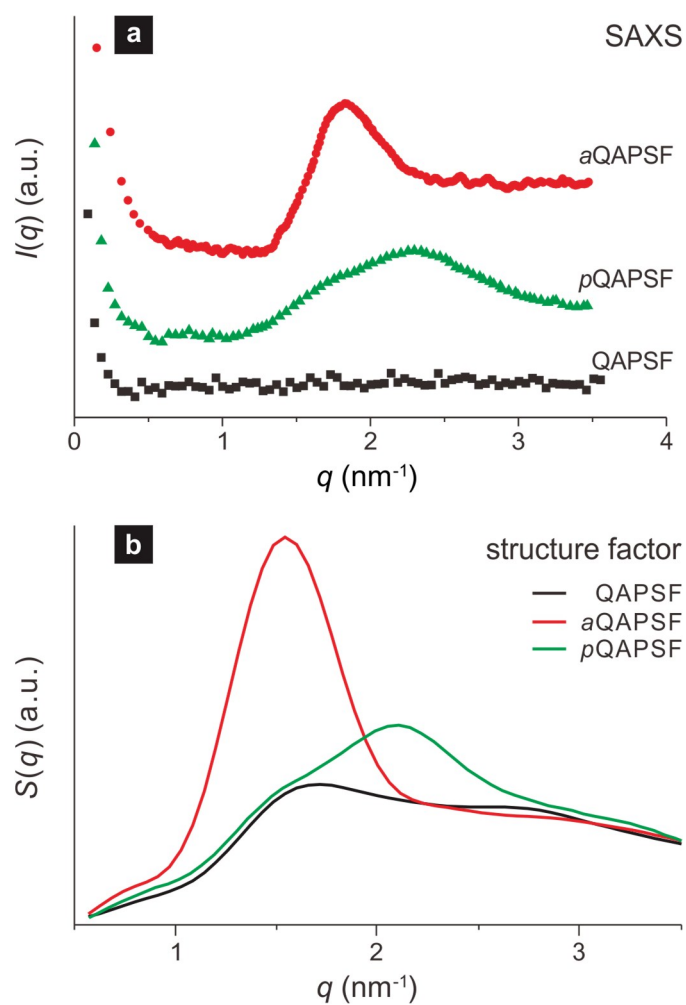


Figure 5. (a) SAXS of QAPSF (IEC = 1.02 mmol/g), aQAPSF (IEC = 0.98 mmol/g), and pQAPSF (IEC = 2.04 mmol/g) membranes at dry state; and (b) structure factors of the hydrophilic species in dry APEs calculated from CGMD simulations.

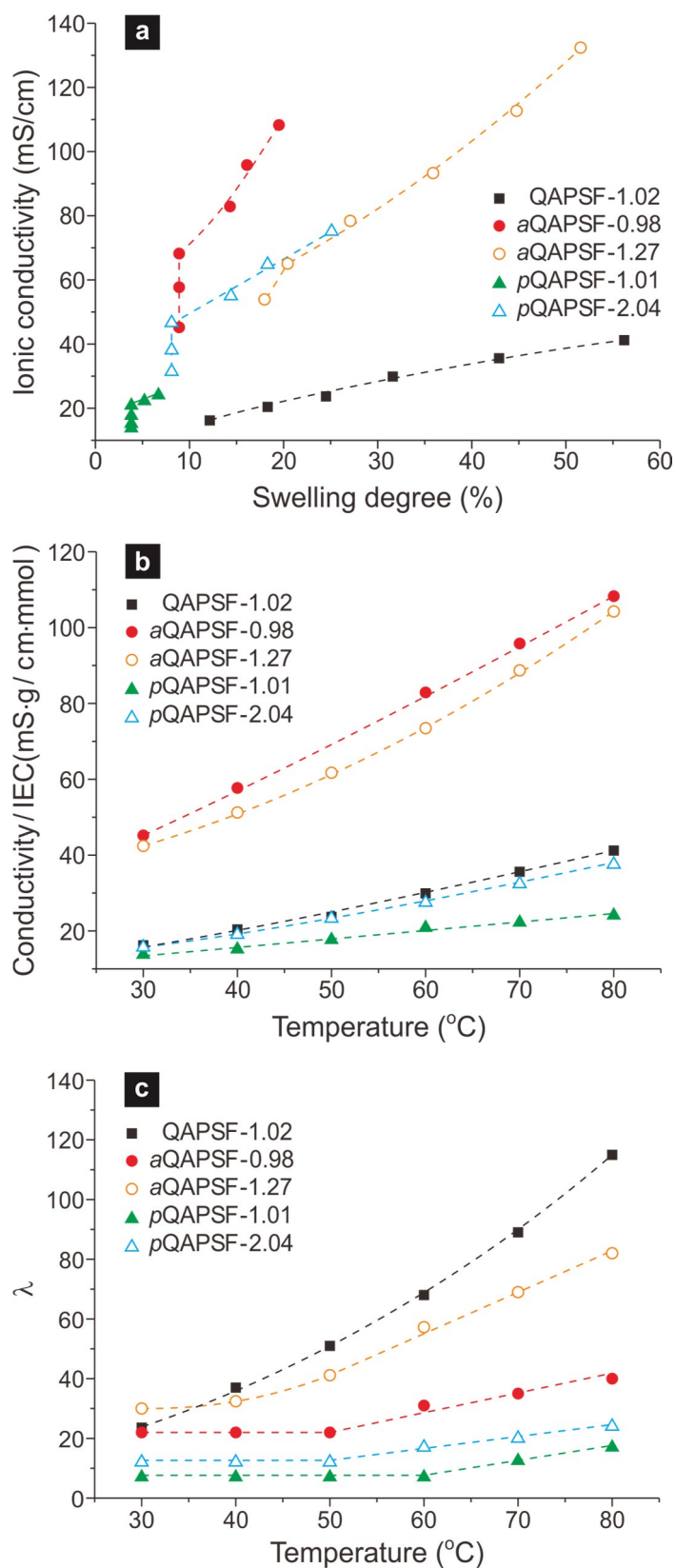


Figure 6. The “ionic conductivity–swelling degree” plot (a), IEC-normalized ionic conductivity (b, conductivity/IEC), and hydration number (c, λ) of PSF-based APE (QAPSF-1.02 (IEC = 1.02 mmol/g), aQAPSF-0.98 (IEC = 0.98 mmol/g), aQAPSF-1.27 (IEC = 1.27

mmol/g), *p*QAPSF-1.01 (IEC = 1.01 mmol/g), and *p*QAPSF-2.04 (IEC = 2.04 mmol/g)) membranes with different IEC at the temperature range of 30 to 80 °C.

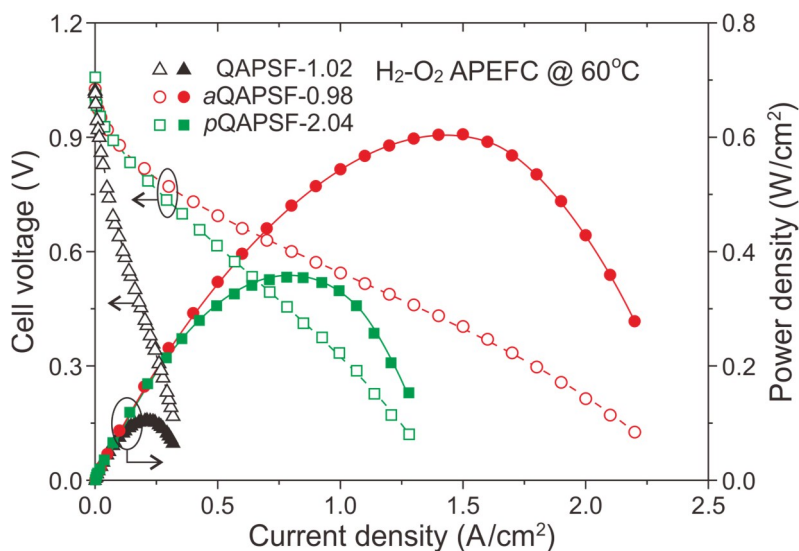


Figure 7. Discharge performances of H₂-O₂ APEFCs based on QAPSF-1.02 (55±5 μm thick, IEC = 1.02 mmol/g), *a*QAPSF-0.98 (55±5 μm thick, IEC = 0.98 mmol/g), and *p*QAPSF-2.04 membranes (55±5 μm thick, IEC = 2.04 mmol/g). The catalysts in both anode and cathode of the APEFCs were Pt/C (60%, Johnson Matthey Co.), with the Pt loading of 0.4 mg/cm². And the weight percentage of QAPSF-1.02, *a*QAPSF-0.98, and *p*QAPSF-2.04 ionomer in the catalyst layers was 20 wt%. Pure H₂ and O₂ gases were fully humidified and fed at a rate of 250 mL/min with 0.1 MPa of back pressure.

Table 2. Physical properties of APEs tested at room temperature.

Sample	DF of CMPSF	IEC ^a (mmol/g)	IEC ^b (mmol/g)	IEC ^c (mmol/g)	σ_{OH^-} (mS/cm)	Swelling degree (%)	Hydration number (λ)
QAPSF-1.02	0.5	1.03	1.06	1.02	16.2	12.1	23
<i>a</i> QAPSF-0.98	1.0	0.92	0.96	0.98	45.2	8.9	22
<i>a</i> QAPSF-1.27	1.5	1.26	1.21	1.27	53.9	18.0	30
<i>p</i> QAPSF-1.01	0.5	1.35	1.05	1.01	13.8	3.8	7
<i>p</i> QAPSF-2.04	1.0	2.24	2.11	2.04	31.4	8.1	12

^a Ideal IEC calculated from polymer composition and the degree of functional group. ^b Real IEC calculated from ¹H NMR.

^c Real IEC tested by titration.

Table 3. Properties of APEs before and after stability test in 1 M NaOH solution at 80°C for 30 days.

Sample	IEC (mmol/g) ^a		OH ⁻ conductivity (mS/cm) ^b	
	before	after	before	after
QAPSF-1.02	1.02	0.35 (↓65.7%)	41.2	13.0 (↓68.4%)
<i>a</i> QAPSF-0.98	0.98	0.81 (↓17.3%)	108.3	85.6 (↓21.0%)
<i>a</i> QAPSF-1.27	1.27	0.90 (↓29.1%)	132.4	91.4 (↓31.0%)
<i>p</i> QAPSF-1.01	1.01	0.89 (↓11.9%)	24.1	20.6 (↓14.5%)
<i>p</i> QAPSF-2.04	2.04	1.73 (↓15.2%)	75.1	62.1 (↓17.3%)

^a Properties measured at room temperature. ^b Properties measured at 80°C.

Varying the Microphase Separation Patterns of Alkaline Polymer Electrolytes

Chen Chen,^a Jing Pan,^{*ab} Juanjuan Han,^{ab} Ying Wang,^a Liang Zhu,^b
Michael A. Hickner,^{*b} and Lin Zhuang^a

^a College of Chemistry and Molecular Sciences, Hubei Key Lab of Electrochemical Power Sources, Wuhan University, Wuhan 430072, China, ^b Department of Materials Science and Engineering, The Pennsylvania State University, University Park, PA 16802, USA

jpan@whu.edu.cn, hickner@matse.psu.edu

TOC

